Upwelling and downwelling behavior in the Elder-Voss-Souza benchmark

Juliette A. Woods[1] and Graham F. Carey[2]

Received 22 January 2006; revised 29 April 2007; accepted 2 July 2007; published 11 December 2007.

[1] The Elder-Voss-Souza (EVS) problem is a standard benchmark for the numerical simulation of variable-density flow and solute transport in a porous medium. However, a review of prior work shows that there is a wide variation in published results on plume structure that cannot entirely be explained by different choices of governing and constitutive equation or by discretization error and numerical error. This work presents results using a new numerical model and algorithms for a series of well-calibrated comparison tests that are designed to elucidate the issue. In addition to the factors mentioned above, we consider the effects of initial and boundary conditions, domain geometry, and problem parameters such as the length of the source boundary segment and the buoyancy parameter in the associated Rayleigh number. It is found that these are key parameters determining the upwelling/downwelling plume behavior. More specifically, the values chosen for the EVS problem lie close to critical values that separate odd and even plume numbers. Consequently, perturbations to the model, mesh, and simulation variables may lead to different plume behavior.

Citation: Woods, J. A., and G. F. Carey (2007), Upwelling and downwelling behavior in the Elder-Voss-Souza benchmark, *Water Resour. Res.*, *43*, W12403, doi:10.1029/2006WR004918.

1. Introduction

[2] The migration of a miscible substance through an aquifer has long been of interest to hydrogeologists and water quality engineers. If the substance is a pollutant, such transport processes may have considerable economic and environmental impact. Thus substantial effort has been put into the numerical simulation of groundwater flow and solute transport to better understand the processes and to provide a reliable predictive capability.

[3] Many pollutants occur at sufficiently high concentrations to substantially alter the density of the groundwater. These pollutants may be due to spills leaching from landfill sites, the spread of saline groundwater, coastal seawater intrusion or leaks from buried waste containers. Gradients in fluid density affect the motion of the groundwater and may lead to more complicated hydrodynamics, including free convection. This is of practical importance as it has been shown that variations in fluid density can spread solute an order of magnitude more quickly than when density differences are neglected [*Simmons and Narayan*, 1997].

[4] Several numerical codes have been developed to solve variable-density groundwater flow and transport, including those described by *Analytic and Computational Research, Inc.* [1994], *Boufadel et al.* [1999a], *Diersch* [1996], *Holzbecher* [1998], *Oldenburg and Pruess* [1995], *Oltean and Buès* [2001], *Frolkovič and de Schepper* [2001] and *Voss* [1984]. One benchmark problem that is frequently used to test these numerical codes is the Elder-Voss-Souza (EVS) problem [*Elder*, 1967; *Voss and Souza*, 1987]. Unfortunately, it has no known analytic solution but it can be used to compare code results qualitatively to experimental observations. This has, in turn, led to cross-code comparisons and there is a remarkable inconsistency in the results obtained in the literature, in which different codes exhibit a variety of flow patterns. These inconsistencies have mainly been attributed to choice of constitutive relations, mesh resolution, and solver tolerances. Nevertheless, despite existing closed-form solutions to alternative test problems, such as those of *Broadbridge et al.* [2002], *Park* [1996], and *van Duijn and Schotting* [1998], the EVS problem has remained one of the standard cases for testing new codes, for example, in work by *Ackerer et al.* [1999], *Boufadel et al.* [1999b], *Kolditz et al.* [1997], *Mazzia et al.* [2001], *Valliappan et al.* [1998], *Voss and Souza* [1987] and others.

[5] A substantial literature exists on the EVS problem. In this study, we focus on the sensitivity issue related to perturbations in the EVS model, discretization and numerical scheme. The outline of the paper is as follows: In the next section we describe the EVS problem and its "peculiarities." Then we formulate a Galerkin finite element (FE) approximation scheme which is used to select a grid density, time-stepping scheme and error tolerance which will be robust. This involves mesh and time step studies to ensure an accurate result on practical meshes of biquadratic elements and accurate solver tolerances. Next, in section 5 we consider specific perturbations and parameter studies for the EVS problem that are designed to elucidate the source of the problem: These include effects due to smoothed boundary

[1]Australian Water Environments, Eastwood, South Australia, Australia.
[2]Institute for Computational Engineering and Sciences, University of Texas at Austin, Austin, Texas, USA.

0043-1397/07/2006WR004918

conditions, different source lengths, domain sizes or Rayleigh numbers. Our results demonstrate that the source of conflicts in simulation results is due to proximity to a critical point that is most easily interpreted physically in terms of the boundary source length in the original EVS problem and illustrated by examining the behavior of the solution for perturbations in source boundary lengths above and below the EVS value. This is then further explored in terms of plume behavior over a range of Rayleigh numbers.

2. Elder-Voss-Souza Problem

[6] The EVS problem has its origins in Elder's laboratory experiment [*Elder*, 1967] for heat-driven convection in a rectangular Hele-Shaw cell that is four times as wide as it is high. The central half of the cell bottom is heated and convection plumes form. A quarter of the way through the laboratory experiment, streamline visualizations show a pattern of six plumes, with four narrow plumes in the center and two larger plumes at the edges; only four plumes remain halfway through the experiment. The direction of rotation is not remarked upon and results are somewhat asymmetric, despite the symmetry of the problem. Elder also provides an approximate numerical solution for a simplified mathematical model of the problem which has provided qualitative base profiles to which other numerical codes have often been compared: however, Elder's numerical results show the development of a single, central plume moving away from the heat source and thus differs from what is observed in his experiment.

[7] The Elder problem was adapted by *Voss and Souza* [1987] to create the EVS problem for solute transport in a porous medium. Two main modifications were made. First, whereas Elder's problem has low-density fluid rising from a heated plate on the lower boundary, the EVS problem has high-density, high-concentration fluid sinking from a constant-concentration source at the top boundary. Thus Elder's results need to be vertically inverted for the purpose of comparison with EVS studies. Secondly, the parameters of Elder's problem are changed to better reflect values found in hydrogeology. The scaling is done such that the Rayleigh number and the problem geometry are preserved. However, it should be noted that the respective heat transfer and porous media models involve different governing equations.

[8] The geometry and parameters of the EVS version of the problem are given in Figure 1 and Table 1. Note that only the concentration has been normalized while the other parameters have physical units of various magnitudes. This problem is simulated by *Voss and Souza* [1987] using the finite element code SUTRA [*Voss*, 1984]. These simulations show a fairly good qualitative agreement with the numerical results of *Elder* [1967], with a single downward central plume of dense solute after 20 years. However, subsequent studies have contested the results of both *Elder* [1967] and *Voss and Souza* [1987] as discussed next.

3. Variations in Numerical Results

[9] Published numerical results vary in the number of plumes and the nature of plume development. Results in the literature are often grouped into two classes that are respectively termed ''upwelling'' and ''downwelling'' solutions, depending on the direction of solute movement in the center of the domain after twenty years. Steady state computations given by *Johannsen* [2003] indicate that different plume structures exist at different problem Rayleigh numbers. However, for the EVS problem with the initial conditions as specified in section 1 and other problem parameters fixed, time-dependent results in the literature show varying numbers of plumes with typically one or two plumes after twenty years. These correspond to ''downwelling'' and ''upwelling'' solutions respectively. In our treatment here an odd number of plumes will correspond to downwelling and an even number to upwelling.

[10] In verification and validation studies, such as the EVS problem, both meshing errors and modeling errors must be considered as reasons for differences in numerical results [*Carey*, 2006]. Inadequate mesh resolution leads to discretization error, while modeling error may be introduced by, say, the choice of a less sophisticated constitutive model. The idea of assessing the mesh error to guide mesh refinement using discretization residuals is being extended to assess model adequacy using model residuals and adjoint techniques. For example, *Carey* [2006] considers automatically assessing both mesh and model choice in this manner) but this technique has not yet been applied to the EVS problem. However, published results to date have used both different mesh resolutions and different model choices.

[11] EVS problem solution differences are known to be due in part to mesh resolution. *Oldenburg and Pruess* [1995] show that a coarse mesh of 1170 nodes, identical to that used by *Voss and Souza* [1987], results in the development of a single plume after 20 years, but finer uniform meshes with 3993 and 5577 nodes respectively show the development of two plumes after 20 years. This pattern is also seen for the finite element code FEFLOW, with coarse meshes yielding downwelling solutions and finer uniform meshes (up to 10,108 nodes) yielding upwelling solutions [*Kolditz et al.*, 1997]. Similar calculations undertaken by *Ackerer et al.* [1999] almost always obtain an upwelling solution, even with a uniform coarse mesh of 1322 nodes. (The one exception is a simulation performed using a deliberately lax convergence criterion.) *Boufadel et al.* [1999b] obtained either a downwelling or an upwelling solution for the same number of nodes (1100), depending on the alignment of their model's triangular elements in this coarse discretization. On the basis of these previous results and further simulations, it is inferred by *Oltean and Buès* [2001] that coarse meshes of 3500 nodes or less can produce either upwellings or downwellings while finer meshes always yield upwellings. However, the finest meshes used to date prior to this study challenge this conclusion of *Oldenburg and Pruess* [1995] and *Oltean and Buès* [2001]. Simulations yielded a downwelling solution for a 4141 node simulation, an upwelling at 16,705 nodes and a downwelling at 66,177 nodes in work by *Frolkovič and de Schepper* [2001] and a similar pattern is obtained by *Diersch and Kolditz* [2002] but for different meshes: a downwelling for a 1105 node mesh, an upwelling for a 4257 node mesh and downwellings for 16,705 and 66,177 node meshes. The EVS problem's extreme sensitivity to small variations in mesh has also been demonstrated by *Carey et al.* [2004]. Hence there remain some questions regarding the sensitivity of the numerical results to the mesh.

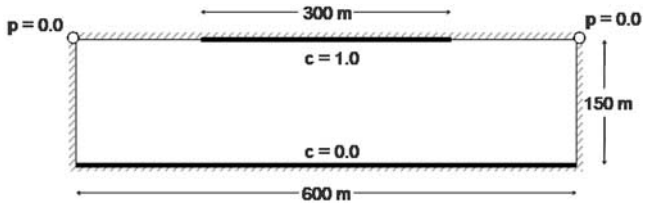

Figure 1. Geometry and boundary conditions of the Elder-Voss-Souza problem.

[12] A second possible reason for such significant qualitative inconsistencies in EVS simulation results is the fact that different governing and constitutive equations have been used. Some, for example, *Elder* [1967] and *Holzbecher* [1998], use a stream function formulation for the fluid flow, or employ a Boussinesq approximation, either of which implies some simplification which may be invalid [*Johannsen*, 2003]. Authors also disagree as to the correct form of Fick's Law, which is used to introduce diffusion and dispersion. Some use $c(\mathbf{v} - \mathbf{v}_{sol}) = -\mathbf{D} \cdot \nabla c$, where c is dimensionless (mass fraction) concentration, $\mathbf{v}$ is the Darcy velocity, $\mathbf{v}_{sol}$ is the velocity of the solute through the medium and D is the dispersivity. Others prefer $C(\mathbf{v} - \mathbf{v}_{sol}) = -\mathbf{D} \cdot \nabla C$, where C is a density-type definition of concentration or "group variable" approach. These two forms of Fick's Law are not equivalent, as can be seen by substituting $C = \rho c$ into $c(\mathbf{v} - \mathbf{v}_{sol}) = -\mathbf{D} \cdot \nabla c$, to obtain $c(\mathbf{v} - \mathbf{v}_{sol}) = -\mathbf{D} \cdot \nabla c - \frac{c}{\rho}\mathbf{D} \cdot \nabla \rho$, which has an additional term when compared to the other form. Moreover, there are differences that arise from the form of the group and individual discretization. Another important difference results from the choice of the constitutive equation describing how density varies with solute concentration. Linear, exponential, quadratic and other functions have all been used [*Lever and Jackson*, 1985; *Holzbecher*, 1998; *Oldenburg and Pruess*, 1995; *Frolkovič and de Schepper*, 2001]. Simulations described by *Woods et al.* [2003] and *Carey et al.* [2004] show that the choice of density equation can visibly alter plume shape (but the number of plumes was unchanged in the one example given). Choices of constitutive equation are known to cause model discrepancies in the simulation of other physical problems [*Carey*, 2006]. However, no clear trends are discernible when published results are grouped together by governing equation.

[13] An important factor is the nonlinearity of the EVS problem and associated instabilities, which can be characterized in part by the Rayleigh number [*Holzbecher*, 1998; *Simpson and Clement*, 2003; *Johannsen*, 2003]. There is an analytic result relating the Rayleigh number to the onset of convection in the related Horton-Rogers-Lapwood (HRL) problem [*Horton and Rogers*, 1945; *Lapwood*, 1948]. The HRL problem is similar to the Elder problem but applies to an infinite strip with constant temperature boundaries. Under these conditions, it can be shown that convective rolls will persist only if $Ra > 4\pi^2 \approx 39.5$. The Elder and EVS problems have a Rayleigh number of 400, an order of magnitude higher than the critical Rayleigh number for the HRL problem, implying a more significant nonlinear effect.

[14] It has been shown that very small changes in the initial conditions can alter the direction of flow [*Frolkovič and de Schepper*, 2001]. Hence the nature and treatment of boundary and initial conditions or integration accuracy may lead to discrepancies in flow structure for different simulators. The initial condition specifies a step function on the middle half of the upper boundary that is approximated in conforming numerical schemes by a continuous function with steep gradient. Differences in the local approximation can cause oscillations. An impulsive "hard start" or an unfavorable choice of time integration scheme and time step may induce local oscillatory behavior. Note that the remainder of the upper boundary condition is impermeable (a Neumann condition) while the middle segment has a specified constant unit concentration (a Dirichlet condition) so there is a singular point where the Neumann and Dirichlet boundary conditions meet. This singularity only exists for concentration; there is no equivalent feature in the pressure field. Simulation results also depend in part on the numerical solution method used. In work by *Woods et al.* [2003] it is shown that even small differences, due to, for instance, mass-lumping, can lead to a change in the direction of the central flow.

[15] Despite the variety of reported results and the problem's evident sensitivity to numerical error, authors such as *Mazzia et al.* [2001] and *Valliappan et al.* [1998] continue to use the EVS problem as a benchmark for testing new codes, usually developing a downwelling with a coarse mesh to match the numerical results of *Elder* [1967] and *Voss and Souza* [1987]. If the EVS problem is to continue to be used for code testing, it is essential that the sources of modeling and numerical sensitivity be identified and understood. This is the main purpose of this paper and the numerical tests are designed to support this reasoning.

4. Formulation of the Present Scheme

[16] The approach used in this study is based on a Galerkin finite element formulation of the coupled nonlinear system for variable-density flow and solute transport. The

Table 1. Elder-Voss-Souza Problem Specifications

	Symbol	Value
Permeability	k	4.845×10^{-13} m^2
Porosity	ε	0.1
Dynamic viscosity	μ	10^{-3} kg m^{-1} s^{-1}
Diffusivity	D	3.565×10^{-6} m^2 s^{-1}
Storativity	S	0
Density change with concentration	β	200 kg m^{-3}
Acceleration due to gravity	g	-9.81 m s^{-2}
Initial conditions		$p(x, y, 0) = \rho(x, y, 0)\ \lvert\mathbf{g}\rvert\ (150 - y)$
		$c(x, y, 0) = 0$
Boundary conditions		$u(0, y, t) = 0$
		$u(600, y, t) = 0$
		$v(x, 0, t) = 0$
		$v(x, 150, t) = 0,\ x \neq 0,\ x \neq 600$
		$p(0, 150, t) = 0$
		$p(600, 150, t) = 0$
		$\partial c/\partial x(0, y, t) = 0$
		$\partial c/\partial x(600, y, t) = 0$
		$c(x, 0, t) = 0$
		$\partial c/\partial y(x, 150, t) = 0,\ 0 \leq x < 150$
		$c(x, 150, t) = 1,\ 150 \leq x \leq 450$
		$\partial c/\partial y(x, 150, t) = 0,\ 450 < x \leq 600$

simulator framework used here has a dial-an-operator structure that allows the user considerable flexibility in the choice of governing and constitutive equations. Thus it permits us to explore the effect of different constitutive models with relative ease. In most of the simulations presented here, we consider the following governing equations on a region Ω with boundary $\partial\Omega$, based on work by *Voss and Souza* [1987]:

$$S\rho\frac{\partial p}{\partial t}+\varepsilon\frac{\partial\rho}{\partial c}\frac{\partial c}{\partial t}+\nabla\cdot(\rho\mathbf{v})=0, \tag{1}$$

$$\varepsilon\rho\frac{\partial c}{\partial t}+\rho\mathbf{v}\cdot\nabla c-\nabla\cdot(\varepsilon\rho\mathbf{D}\nabla c)=0, \tag{2}$$

$$\mathbf{v}=-\frac{\mathbf{k}}{\mu}(\nabla p-\rho\mathbf{g}), \tag{3}$$

$$\rho=\rho_0+\beta c. \tag{4}$$

where S is storativity, ε is porosity and $\mathbf{D}$ is the hydrodynamic dispersion coefficient incorporating both molecular diffusivity and hydrodynamic dispersivity; k is permeability, μ is viscosity, $\mathbf{g}$ is acceleration due to gravity, ρ_0 is the fluid density when $c=0$, $\rho_{\max}$ is the density at $c=1$ and β is a specified coefficient derived from experiment [*Holzbecher*, 1998]. The hydrodynamic dispersion coefficient $\mathbf{D}$ is commonly described using the Bear-Scheidegger equations [*Bear*, 1961; *Scheidegger*, 1961], but the EVS problem incorporates no hydrodynamic dispersivity so $\mathbf{D}$ reduces to a scalar, the molecular diffusivity.

[17] The pressure boundary conditions are

$$p(\mathbf{x},t)=\hat{p}(\mathbf{x}),\quad \mathbf{x}\in\partial\Omega_{p1},\qquad \rho\mathbf{v}\cdot\mathbf{n}=\hat{\sigma}_p(\mathbf{x}),\quad \mathbf{x}\in\partial\Omega_{p2}, \tag{5}$$

for $\partial\Omega=\partial\Omega_{p1}\cup\partial\Omega_{p2}$, where $\hat{p}(\mathbf{x})$ and $\hat{\sigma}_p(\mathbf{x})$ are known functions and $\mathbf{n}$ is the unit normal to the surface. Similarly, the boundary conditions for concentration are

$$c(\mathbf{x},t)=\hat{c}(\mathbf{x}),\quad \mathbf{x}\in\partial\Omega_{c1},\qquad \varepsilon\rho\mathbf{D}\nabla c\cdot\mathbf{n}=\hat{\sigma}_c(\mathbf{x}),\quad \mathbf{x}\in\partial\Omega_{c2}, \tag{6}$$

for $\partial\Omega=\partial\Omega_{c1}\cup\partial\Omega_{c2}$, where $\hat{c}(\mathbf{x})$ and $\hat{\sigma}_c(\mathbf{x})$ are known.

[18] The initial conditions in Ω are

$$p(x,\,y,\,0)=p_0(x,\,y),\qquad c(x,\,y,\,0)=c_0(x,\,y), \tag{7}$$

where functions $p_0(x, y)$ and $c_0(x, y)$ are known.

[19] Introducing test functions q and w in a weighted-residual statement for (1) and (2) and applying Gauss' divergence theorem, we obtain

$$\int_\Omega S\rho\frac{\partial p}{\partial t}q\,d\mathbf{x}+\int_\Omega\varepsilon\frac{\partial\rho}{\partial c}\frac{\partial c}{\partial t}q\,d\mathbf{x}-\int_\Omega\rho\mathbf{v}\cdot\nabla q\,d\mathbf{x}+\int_{\partial\Omega}\rho q(\mathbf{v}\cdot\mathbf{n})\,d\mathbf{s}=0, \tag{8}$$

$$\int_\Omega\varepsilon\rho\frac{\partial c}{\partial t}w\,d\mathbf{x}+\int_\Omega(\rho\mathbf{v}\cdot\nabla c)w\,d\mathbf{x}+\int_\Omega\varepsilon\rho\mathbf{D}\nabla c\cdot\nabla w\,d\mathbf{x}-\int_{\partial\Omega}\varepsilon\rho\mathbf{D}\nabla c\cdot\mathbf{n}w\,d\mathbf{s}=0, \tag{9}$$

[20] Darcy's law (3) is substituted into (8)–(9). After rearranging, the problem becomes: Find p and c satisfying the initial conditions, essential boundary conditions $p=\hat{p}$ on $\partial\Omega_{p1}$ and $c=\hat{c}$ on $\partial\Omega_{c1}$ and such that

$$\int_\Omega S\rho\frac{\partial p}{\partial t}q\,d\mathbf{x}+\int_\Omega\frac{\mathbf{k}}{\mu}\rho(\nabla p\cdot\nabla q)\,d\mathbf{x}=-\int_\Omega\varepsilon\frac{\partial\rho}{\partial c}\frac{\partial c}{\partial t}q\,d\mathbf{x}-\int_\Omega\frac{\mathbf{k}}{\mu}\rho^2(\mathbf{g}\cdot\nabla q)\,d\mathbf{x}-\int_{\partial\Omega_{p2}}\hat{\sigma}_pq\,d\mathbf{s} \tag{10}$$

$$\int_\Omega\varepsilon\rho\frac{\partial c}{\partial t}w\,d\mathbf{x}-\int_\Omega\frac{\mathbf{k}}{\mu}\rho(\nabla p\cdot\nabla c)w\,d\mathbf{x}+\int_\Omega\frac{\mathbf{k}}{\mu}\rho^2(\mathbf{g}\cdot\nabla c)w\,d\mathbf{x}+\int_\Omega\varepsilon\rho\mathbf{D}(\nabla c\cdot\nabla w)\,d\mathbf{x}=\int_{\partial\Omega_{c2}}\hat{\sigma}_cw\,d\mathbf{s}. \tag{11}$$

hold for all admissible test functions q and w where $q=0$ on $\partial\Omega_{p1}$ and $w=0$ on $\partial\Omega_{c1}$.

[21] The finite element formulation for (10)–(11) follows on introducing the approximation subspaces for pressure and concentration to obtain: find (p_h, c_h) with p_h and c_h satisfying the essential boundary conditions and initial conditions and such that the corresponding approximate integral equations are satisfied for all admissible test functions q_h and w_h where $q_h=0$ on $\partial\Omega_{p1}$ and $w_h=0$ on $\partial\Omega_{c1}$.

[22] Introducing a finite element discretization and basis to define the associated trial and test subspaces leads to a sparse coupled nonlinear semidiscrete system of ODEs of the form

$$\mathbf{M}^p\dot{\mathbf{p}}+\mathbf{K}^p\mathbf{p}=\mathbf{F}^p,\qquad \mathbf{M}^c\dot{\mathbf{c}}+\mathbf{K}^c\mathbf{c}=\mathbf{F}^c, \tag{12}$$

where

$$M^p_{ij}=\int_\Omega S\rho_h\phi_i\phi_j\,d\mathbf{x}, \tag{13}$$

$$K^p_{ij}=\int_\Omega\frac{\mathbf{k}}{\mu}\rho_h\left(\nabla\phi_i\cdot\nabla\phi_j\right)d\mathbf{x}, \tag{14}$$

$$F^p_i=-\int_\Omega\left[\varepsilon\frac{\partial\rho_h}{\partial c_h}\frac{\partial c_h}{\partial t}\phi_i+\frac{k}{\mu}\rho_h^2(\mathbf{g}\cdot\nabla\phi_i)\right]d\mathbf{x}+\int_{\partial\Omega_{p2}}\hat{\sigma}_p\phi_i\,d\mathbf{s}, \tag{15}$$

$$M^c_{ij}=\int_\Omega\varepsilon\rho_h\phi_i\phi_j\,d\mathbf{x}, \tag{16}$$

$$K_{ij}^c = \int_\Omega \left[-\rho_h \frac{k}{\mu} \{ (\nabla p_h - \rho_h \mathbf{g}) \cdot \nabla \phi_j \} \phi_i + \varepsilon \rho_h \mathbf{D}_h (\nabla \phi_i \cdot \nabla \phi_j) \right] d\mathbf{x}, \tag{17}$$

$$F_i^c = \int_{\partial \Omega_{c2}} \hat{\sigma}_c \phi_i \, d\mathbf{s}, \tag{18}$$

and $\rho_h = \rho(c_h)$. Here we have used the same finite element basis for both pressure and concentration approximations and the dependence of density on concentration is specified as in (4). Tensor-product biquadratic quadrilateral elements are used in the later simulations. The above systems (12) are coupled nonlinearly through various terms as implied in (13)–(18). Note that (12) can be integrated and solved either in fully coupled or decoupled form in various ways. In the present work, we iteratively decouple within each time step and lag ρ and c in (13)–(15) and lag ρ and p in (16)–(18).

4.1. Solution Algorithm

[23] For a general time step $n + 1$, the system is integrated with respect to time using the Adams-Bashford/Trapezoidal (ABTR) predictor-corrector method. However, for reasons of computational efficiency, our implementation of ABTR involves history vectors $\dot{\mathbf{p}}$ and $\dot{\mathbf{c}}$, so an initialization phase is required. Thus our algorithm proceeds as follows.

4.1.1. First Time Step ($n = 0$)

[24] An implicit backward Euler scheme is used because it requires no history vectors and suppresses numerical oscillations. A small time step ensures accuracy. The backward Euler scheme is

$$\left(\frac{1}{\Delta t_n} \mathbf{M}^p + \mathbf{K}^p \right) \mathbf{p}_{n+1}^{BE} = \mathbf{F}^p + \frac{1}{\Delta t_n} \mathbf{M}^p \mathbf{p}_n, \tag{19}$$

$$\left(\frac{1}{\Delta t_n} \mathbf{M}^c + \mathbf{K}^c \right) \mathbf{c}_{n+1}^{BE} = \mathbf{F}^c + \frac{1}{\Delta t_n} \mathbf{M}^c \mathbf{c}_n, \tag{20}$$

where $\Delta t_n = t_{n+1} - t_n$ is the length of the step.

[25] History vectors $\dot{\mathbf{p}}$ and $\dot{\mathbf{c}}$ are then calculated using

$$\dot{\mathbf{p}}_{n+1} = \frac{1}{\Delta t_n} (\mathbf{p}_{n+1} - \mathbf{p}_n), \qquad \dot{\mathbf{c}}_{n+1} = \frac{1}{\Delta t_n} (\mathbf{c}_{n+1} - \mathbf{c}_n). \tag{21}$$

4.1.2. Second and Third Time Steps ($n = 1, 2$)

[26] The backward Euler scheme (19)–(20) is again used, but now as a corrector in combination with a preceding forward Euler predictor step that provides a computationally inexpensive initial estimate of the solution to help treat the nonlinearities. This is similar to the forward Euler/backward Euler (FEBE) predictor-corrector strategy, described by *Gresho and Sani* [1998]. The forward Euler scheme is

$$\frac{1}{\Delta t_n} \mathbf{M}^p \mathbf{p}_{n+1}^{FE} = \frac{1}{\Delta t_n} \mathbf{M}^p \mathbf{p}_n + (\mathbf{F}^p - \mathbf{K}^p \mathbf{p}_n), \tag{22}$$

$$\frac{1}{\Delta t_n} \mathbf{M}^c \mathbf{c}_{n+1}^{FE} = \frac{1}{\Delta t_n} \mathbf{M}^c \mathbf{c}_n + (\mathbf{F}^c - \mathbf{K}^c \mathbf{c}_n), \tag{23}$$

so applying (12),

$$\frac{1}{\Delta t_n} \mathbf{M}^p \mathbf{p}_{n+1}^{FE} = \frac{1}{\Delta t_n} \mathbf{M}^p \mathbf{p}_n + \mathbf{M}^p \dot{\mathbf{p}}_n, \tag{24}$$

$$\frac{1}{\Delta t_n} \mathbf{M}^c \mathbf{c}_{n+1}^{FE} = \frac{1}{\Delta t_n} \mathbf{M}^c \mathbf{c}_n + \mathbf{M}^c \dot{\mathbf{c}}_n. \tag{25}$$

Thus (22)–(23) can be implemented in a computationally 423
inexpensive form as

$$\mathbf{p}_{n+1}^{FE} = \mathbf{p}_n + \Delta t_n \dot{\mathbf{p}}_n, \qquad \mathbf{c}_{n+1}^{FE} = \mathbf{c}_n + \Delta t_n \dot{\mathbf{c}}_n, \tag{26}$$

since the history vectors are known from (21).

4.1.3. Fourth and Subsequent Time Steps

[27] The Adams-Bashford/Trapezoidal (ABTR) predictor-corrector scheme is used [*Gresho and Sani*, 1998] with the Adams-Bashford predictor step,

$$\mathbf{p}_{n+1}^{AB} = \mathbf{p}_n + \frac{\Delta t_n}{2} \left[\left(2 + \frac{\Delta t_n}{\Delta t_{n-1}} \right) \dot{\mathbf{p}}_n - \left(\frac{\Delta t_n}{\Delta t_{n-1}} \right) \dot{\mathbf{p}}_{n-1} \right], \tag{27}$$

$$\mathbf{c}_{n+1}^{AB} = \mathbf{c}_n + \frac{\Delta t_n}{2} \left[\left(2 + \frac{\Delta t_n}{\Delta t_{n-1}} \right) \dot{\mathbf{c}}_n - \left(\frac{\Delta t_n}{\Delta t_{n-1}} \right) \dot{\mathbf{c}}_{n-1} \right], \tag{28}$$

and the trapezoidal rule corrector,

$$\frac{2}{\Delta t_n} \mathbf{M}^p \mathbf{p}_{n+1} + \mathbf{K}^p \mathbf{p}_{n+1} = \mathbf{F}^p + \frac{2}{\Delta t_n} \mathbf{M}^p \mathbf{p}_n + \mathbf{M}^p \dot{\mathbf{p}}_n, \tag{29}$$

$$\frac{2}{\Delta t_n} \mathbf{M}^c \mathbf{c}_{n+1} + \mathbf{K}^c \mathbf{c}_{n+1} = \mathbf{F}^c + \frac{2}{\Delta t_n} \mathbf{M}^c \mathbf{p}_c + \mathbf{M}^c \dot{\mathbf{p}}_n, \tag{30}$$

where the history vectors are calculated using

$$\begin{aligned} \dot{\mathbf{p}}_n &= \frac{2}{\Delta t_{n-1}} (\mathbf{p}_n - \mathbf{p}_{n-1}) - \dot{\mathbf{p}}_{n-1}, \\ \dot{\mathbf{c}}_n &= \frac{2}{\Delta t_{n-1}} (\mathbf{c}_n - \mathbf{c}_{n-1}) - \dot{\mathbf{c}}_{n-1}. \end{aligned} \tag{31}$$

4.1.4. Solution of Algebraic Systems

[28] Depending on the time step, nonlinear coupled algebraic systems (19)–(20) or (29)–(30) need to be solved. The pressure equation is solved first and the result is substituted into the equation for concentration which is then solved. These steps are repeated until the following convergence criteria are met:

$$\begin{aligned} \frac{\| \mathbf{p}_{n+1(l+1)} - \mathbf{p}_{n+1(l)} \|}{\| \mathbf{p}_{n+1(l+1)} \|} &< \epsilon_{p,nonlinear}, \\ \frac{\| \mathbf{c}_{n+1(l+1)} - \mathbf{c}_{n+1(l)} \|}{\| \mathbf{c}_{n+1(l+1)} \|} &< \epsilon_{c,nonlinear}, \end{aligned} \tag{32}$$

where the subscript in brackets refers to the nonlinear iteration number and the tolerances ϵ are user-specified to ensure that the nonlinearities are resolved.

[29] The resulting linear algebraic systems arising at each decoupling step above are solved iteratively using a BCG algorithm with an ILU preconditioner [*Barrett et al.*, 1994].

Table 2. Grid l Levels of *Frolkovič and de Schepper* [2001] Defined for the Half-Domain

	Linear Elements		Quadratic Elements	
l	Length × Width	Total	Length × Width	Total
4	32 × 16	512	16 × 8	128
5	64 × 32	2048	32 × 16	512
6	128 × 64	8192	64 × 32	2048
7	256 × 128	32768	128 × 64	8192
8	512 × 256	131,072	256 × 128	32768

The stopping tests for these linear solves are

$$\frac{\|\mathbf{z}^p_{[j]}\|}{\|\mathbf{z}^p_{[0]}\|} < \epsilon_{p,linear}, \quad \frac{\|\mathbf{z}^c_{[j]}\|}{\|\mathbf{z}^c_{[0]}\|} < \epsilon_{c,linear}, \tag{33}$$

where the subscript in square brackets refers to the linear solver iteration and

$$\mathbf{z}^p_{[j]} = (\mathbf{Q}^p)^{-1}\left(\mathbf{K}^p\mathbf{p}_{n+1[j]} - \mathbf{F}^p\right),$$
$$\mathbf{z}^c_{[j]} = (\mathbf{Q}^c)^{-1}\left(\mathbf{K}^c\mathbf{c}_{n+1[j]} - \mathbf{F}^c\right), \tag{34}$$

where $\mathbf{Q}$ is the preconditioning matrix. The solution scheme can be implemented on a single processor, or in parallel following the approach described by *Carey et al.* [1999]. The time step can be fixed to a user-specified value or (by default) selected adaptively on the basis of the difference in predictor and corrector iterates.

5. Numerical Experiments

[30] We now investigate the plume structure issue for the EVS problem using the scheme described in section 4. All simulations are run using the ABTR predictor-corrector time-integration scheme for the model in equations (1)–(4). Because of the symmetry of the EVS problem, only the left-hand side of the domain is simulated, with a flux symmetry boundary condition on the symmetric centerline $x = 300$. This is a common choice for efficiently calculating EVS results and is appropriate for our purpose here. The first part of our numerical investigation with the accurate finite element model explores various sources of perturbations to which the EVS problem appears to exhibit plume sensitivity. The second part includes additional experiments demonstrating the role of proximity to the critical point through variations of boundary segment/domain length scales and the buoyancy parameter β.

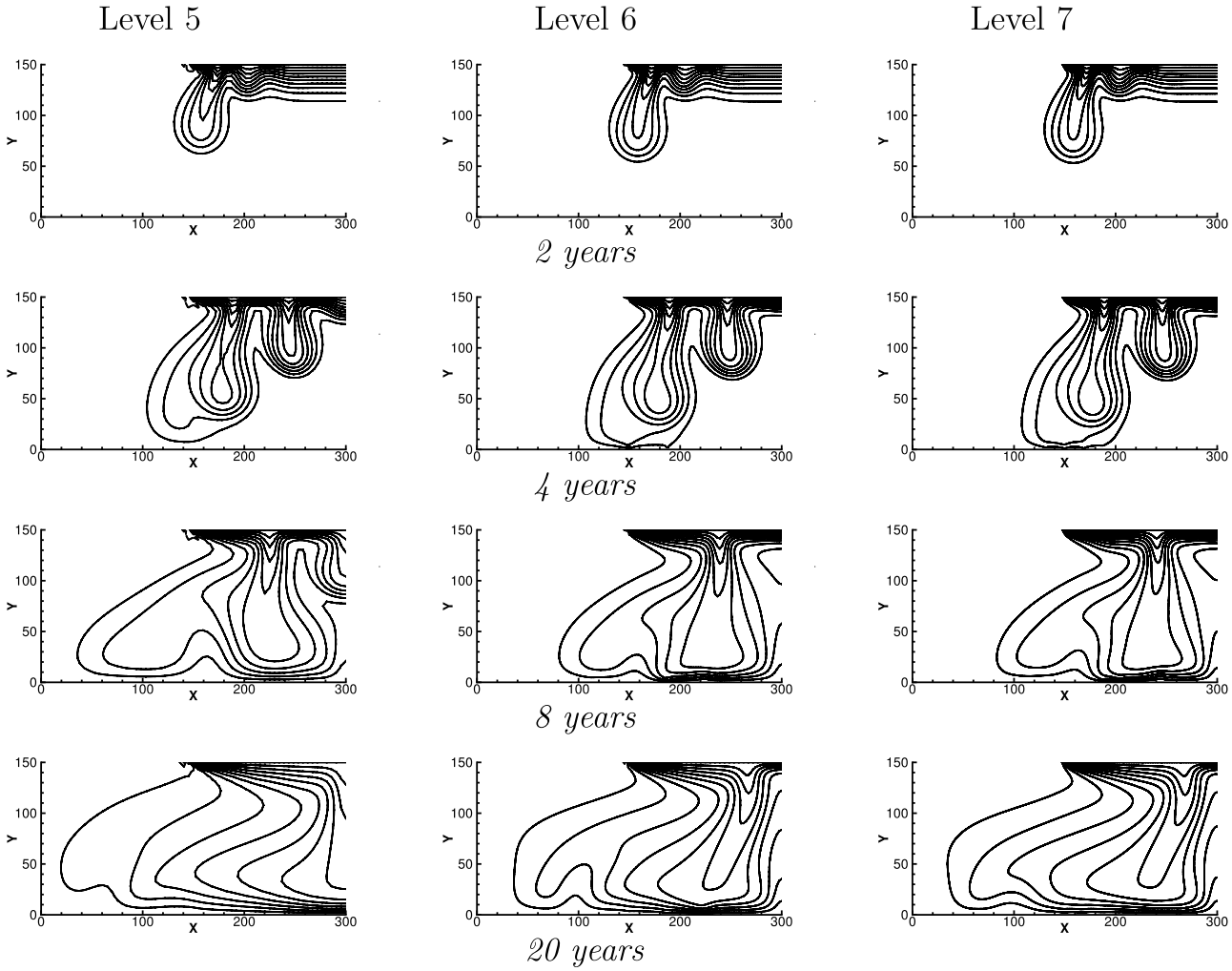

Figure 2. Concentration contours for grid levels 5, 6, and 7.

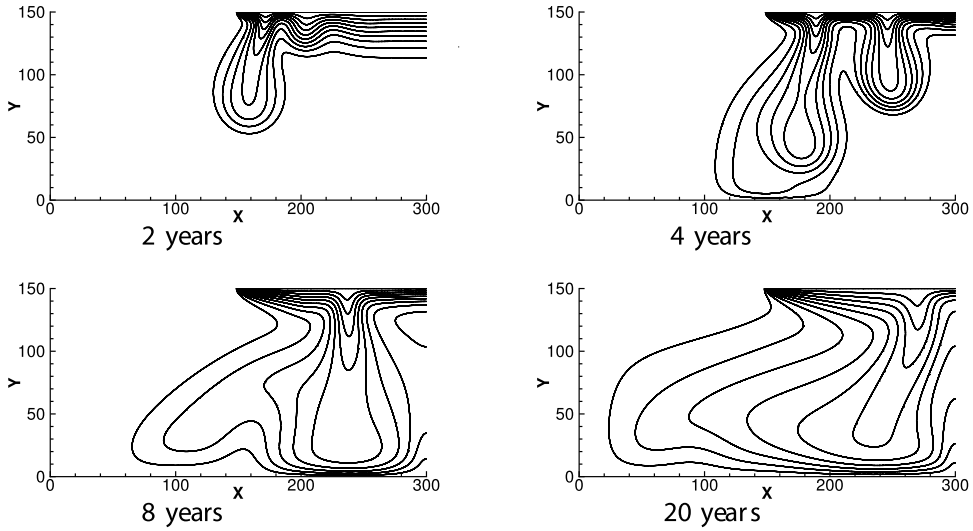

Figure 3. Concentration contours for grid level 8.

5.1. Choice of Discretization and Error Tolerances

[31] First, appropriate spatial and temporal discretizations and error tolerances must be established, so that later simulations of EVS variations are performed under consistent and robust numerical conditions. Different error tolerances were considered by running the EVS problem on a 64×32 element grid and a 128×64 element grid of biquadratic elements with uniform time steps. It was found that when $\epsilon_{linear} = \epsilon_{nonlinear} = 10^{-4}$ or 10^{-5}, results were essentially identical, but that an error tolerance of 10^{-3} led to different flow behavior. An error tolerance of 10^{-4} was therefore chosen as both accurate and computationally efficient. Time steps of 1, 5, 10, 20 or 40 steps per year were also considered. Only the 1 step per year simulation had results which differed significantly from the others. A conservative choice of time step of 40 steps per year was chosen.

[32] The EVS problem was run on four different meshes, according to the grid level scheme of *Frolkovič and de Schepper* [2001] as given in Table 2. (Since we are using biquadratic elements, our results will be much more accurate for the same element partition using their choice of linear elements).

[33] Contour plots after 2, 4, 8 and 20 years are given in Figure 2 for grid levels 5–7. Figure 3 gives the results for grid level 8 at a larger scale for clearer viewing. (Contours range from 0.1 to 0.9 at intervals of 0.1; this is true of all contour plots given in this article.) After two years, level 5 differs from the others in that the outer plume is slightly shorter. At four years, the level 5 simulation is starting to develop a central plume (it has become a "downwelling" case) while levels 6–8 are upwelling cases, with no central plume. Levels 6, 7 and 8 agree well with each other, although there are small differences. These are most obvious at 20 years, where the level 6 grid shows a steep bend in the contours close to coordinates (100,0); this bend is weaker in the results for the level 7 grid and is weaker yet in the grid level 8 simulation. However, the results produced by level 7 and level 8 grids are sufficiently similar that level 7 is selected for the majority of the simulations which follow. Note that this result at 20 years does not agree with the results of *Frolkovič and de Schepper* [2001] using lower degree approximation on the same mesh. However, our results are with higher degree elements and a much finer mesh of linear elements would be required to obtain comparable accuracy.

5.2. Smoothed Initial and Boundary Conditions

[34] Next we consider the effect of regularizing the concentration boundary and initial conditions. More specifically, instead of implementing a step function form of the initial and boundary conditions, the concentration is smoothed using a double-quadratic function such that on the left half-domain,

$$c_x(x) = \begin{cases} 0, & x < 150 - l, \\ 0.5\left(\dfrac{x - 150 + l}{l}\right)^2, & 150 - l \le x \le 150, \\ 0.5 + \left(\dfrac{x - 150}{l}\right) - 0.5\left(\dfrac{x - 150}{l}\right)^2, & 150 \le x \le 150 + l, \\ 1, & 150 + l \le x, \end{cases} \tag{35}$$

where l is a user-specified "smoothing width" and

$$c_y(y) = \begin{cases} 0, & y < 150 - 2l, \\ 0.5\left(\dfrac{y - 150 + 2l}{l}\right)^2, & 150 - 2l \le y \le 150 - l, \\ 0.5 + \left(\dfrac{y - 150 + l}{l}\right) - 0.5\left(\dfrac{y - 150 + l}{l}\right)^2, & 150 - l \le y \le 150, \end{cases} \tag{36}$$

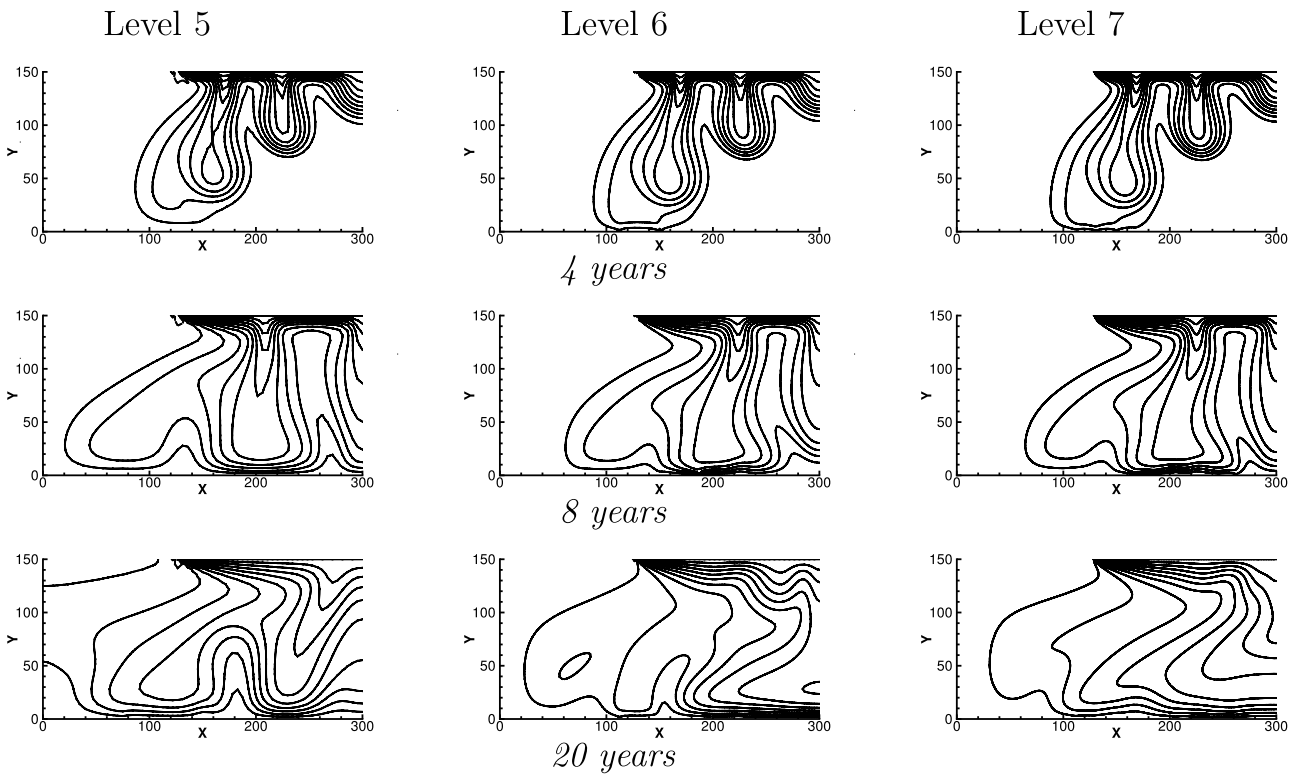

Figure 4. Concentration contours for the smoothed boundary condition version of the EVS problem.

The initial conditions are set to be $c(x, y, 0) = c_x(x) \cdot c_y(y)$. These functions are chosen because the resulting initial conditions are continuous and have derivatives which approach zero at the edges of the smoothed zone. This physically corresponds to a slightly infiltrated zone at the mesh scale. For our simulation runs, the smoothing width is as wide as a level 5 mesh element, i.e., $l = 9.375$ m. The aim here is to see whether a variation on the EVS problem with smoothed initial and boundary conditions has results which are more consistent between grid levels than the EVS problem. Grid levels 5, 6 and 7 are considered.

[35] Concentration contours at two years differ little from those produced by the regular EVS problem of Figure 2 and are not shown. However, at 4 years there are significant differences between the smoothed boundary condition results in Figure 4 and corresponding regular cases in Figure 2 as a central plume has now developed for all smooth boundary condition simulations. At year 8, the smoothed boundary condition simulations for grid levels 6 and 7 have produced downwelling solutions, while the regular EVS produces upwelling solutions for these grids. Results at 8 years look similar for all grid levels, except that the outermost plume of the level 5 grid simulation extends further to the left. Remarkably, at 20 years, the level 5 grid simulation changes from a downwelling solution to an upwelling solution and the level 6 grid and level 7 grid solutions are dissimilar despite both being downwelling solutions. Clearly, our perturbation of the upper constant concentration boundary has significantly affected solution results. The local smoothing has not decreased the problem's sensitivity, but the number of plumes at 4 years has increased. As introducing the smoothing process can also be viewed in terms of modifying the "effective" length of the applied upper constant-concentration boundary condition, this observation suggests that the length of this boundary segment may be important to resolving the sensitivity of the EVS problem with regard to the number of plumes. Accordingly, we proceed next to examine this key issue in a series of numerical experiments.

5.3. Stability and Source Length Scale

[36] The analogy to instability problems in other coupled flow problems suggests that a factor warranting investigation is the relative length of the forcing boundary segment. In the EVS problem this is the upper concentration source length boundary, which we denote L. The standard EVS model source length is 300 m (in the full domain) and in the next set of simulations the source length is varied from 100 m to 500 m. In a practical sense this may be viewed as a type of simple design issue that would be considered in designing a holding pond for effluent of greater density than the underlying groundwater or for an artificial basin designed to slowly release its contents (such as Australia's salt disposal basins). However, our central interest here is on the sensitivity of plume structure to the length of the source boundary.

[37] Concentration contours are given in Figures 5 and 6 for simulations conducted using the level 7 grid (the 100-m case is omitted for reasons of space). Plume initiation starts at the edge of this segment on the boundary and then spreads inward over time until the line of symmetry is reached, after which the plumes begin to merge. Most cases result in one or two plumes over the full domain after twenty years, but the $L = 500$ case has three plumes remaining at that time. When $L = 500$, the simulation results start to resemble the flow structures arising from instabilities

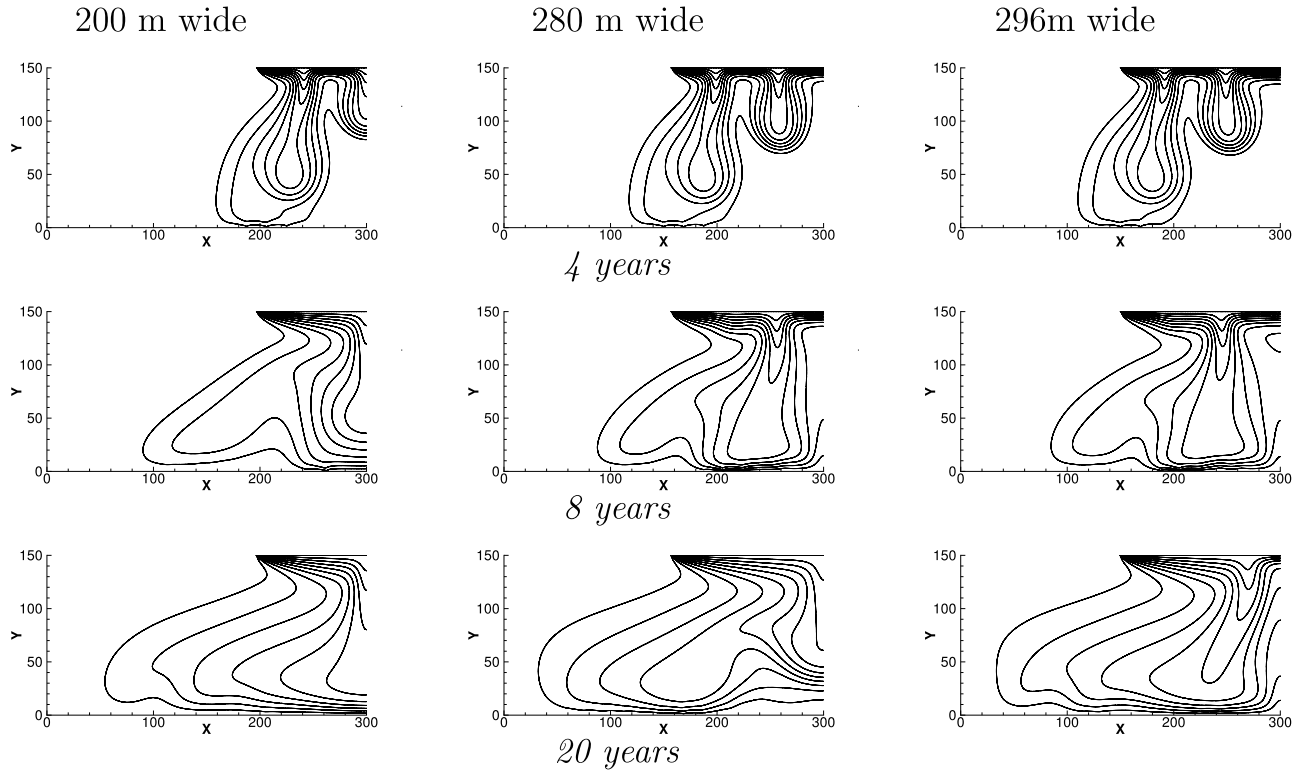

Figure 5. Concentration contours for shorter upper source boundary lengths.

in similar systems such as the classical Rayleigh-Benard problem [see, e.g., *Chandrasekhar*, 1981; *Rayleigh*, 1916].

[38] Year-by-year plots of the simulations show that the number of small plumes which develop along the source line before the line of symmetry is reached increases with source width L (J. A. Woods and G. F. Carey, An investigation of the Elder-Voss-Souza problem with high resolution benchmark simulations, technical report in preparation

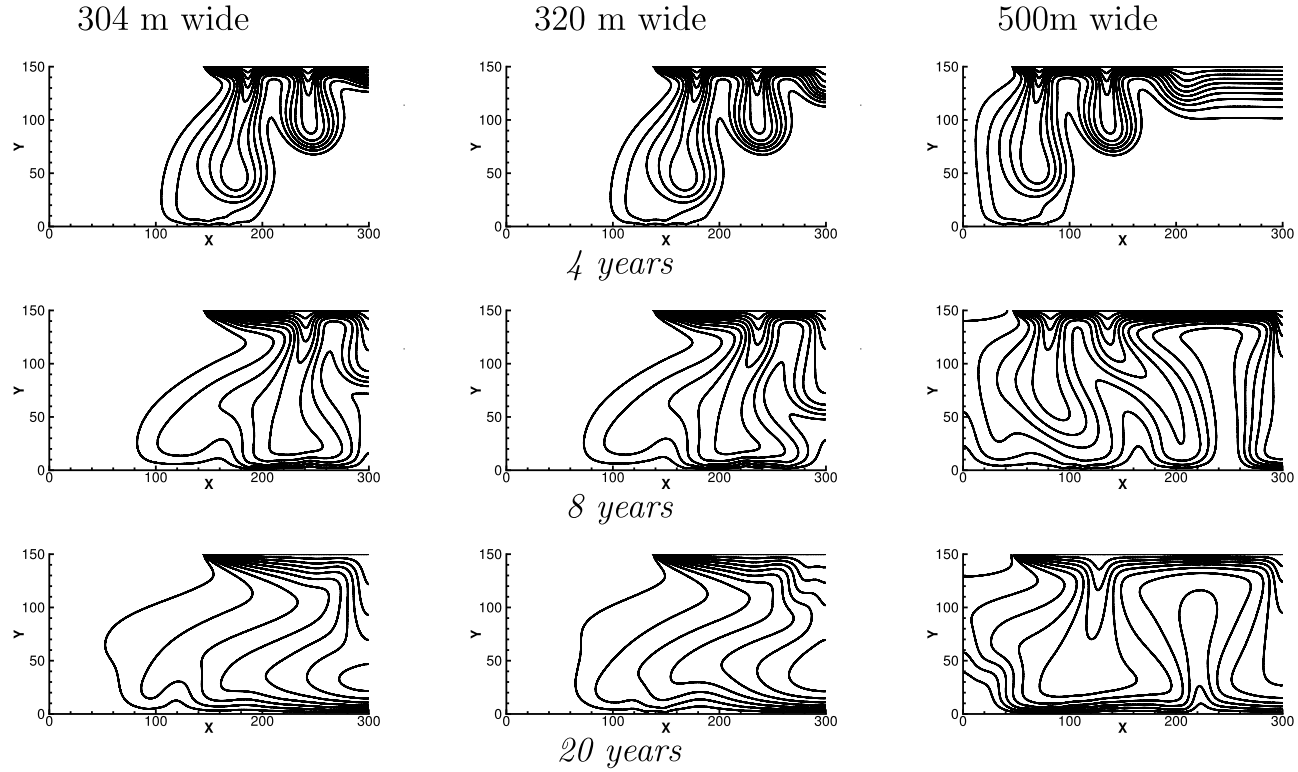

Figure 6. Concentration contours for longer upper source boundary lengths.

WOODS AND CAREY: THE ELDER-VOSS-SOUZA BENCHMARK

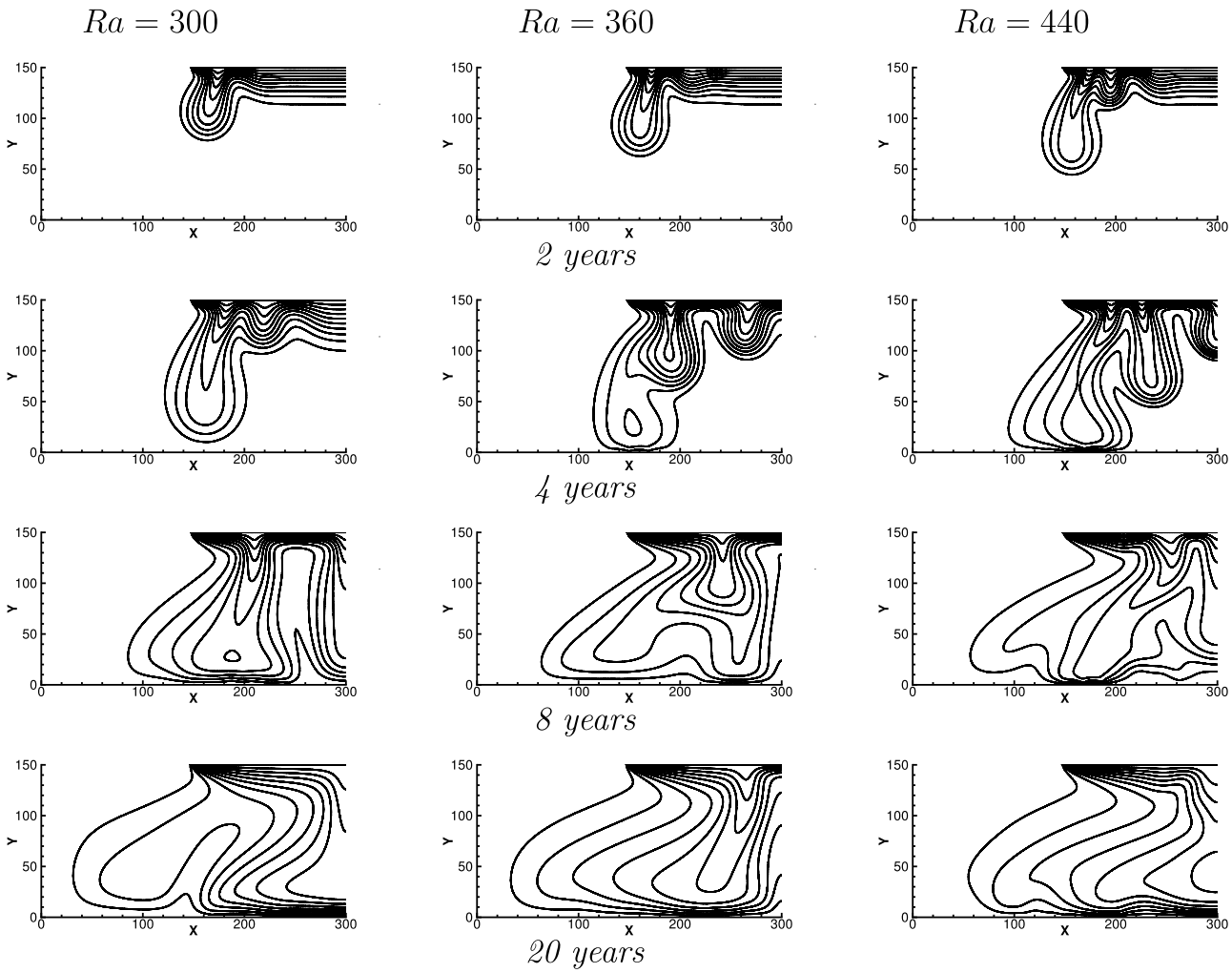

Figure 7. Concentration contours for grid level 7 for various Rayleigh numbers.

for Institute for Computational Engineering and Sciences, University of Texas, Austin, 2007) (hereinafter referred to as Woods and Carey, manuscript in preparation, 2007). Moreover, for most of the cases investigated, an odd number of small plumes in this phase correlates with a downwelling solution; an even number of small plumes correlates with an upwelling solution.

[39] More generally, the results show that there exist critical source widths (L) corresponding to transitions between one, two and three plume solutions. In particular, a simulation with a slightly narrower upper concentration source length (L = 296) than the EVS standard of L = 300 leads stably to an upwelling while a slightly wider boundary (L = 304) leads stably to a downwelling; so the standard EVS problem source length lies close to the critical point between these two flow behaviors. This explains why the problem is so sensitive to modeling and simulation error. If the width is close to a critical value, then other errors due to mesh, solver tolerance, constitutive model discrepancy etc may induce a shift to the wrong plume structure (see *Barth and Carey* [2006] for analysis of a 3D heated fluid experiment and simulation results where a similar discrepancy arises near a critical point). In a sense, the problem is a suitable demanding test case to determine robustness of methods, presuming that a high-resolution reliable benchmark is available for the verification comparison.

5.4. Varying Buoyancy Parameter β

[40] We now consider whether plume structure is sensitive to changes in the nonlinearity of the governing equations due to buoyancy. This was explored by varying buoyancy parameter value β. Values of 150, 180, 195, 200, 205, 220 and 250 (corresponding to Rayleigh numbers of 300, 360, 390, 400, 410, 440, and 500) were considered on level 7 grids. Representative results are given in Figure 7. At two years, both the length of the outer plume and the number of forming plumes increases with β (or equivalent *Ra*). Consider the number of plumes in the full domain (i.e., when the half-domain simulated is reflected across the right-hand boundary representing the line of symmetry). For β = 150 (*Ra* = 300), there are two long plumes and two small plumes just forming, while the β = 180 (*Ra* = 360) case

shows signs of a central fifth plume starting. For $\beta = 220$ ($Ra = 440$), there are five plumes in the full domain and the $\beta = 250$ ($Ra = 500$) case (not shown) has six plumes in the full domain. At eight years, the $\beta = 150$ ($Ra = 300$) and $\beta = 220$ ($Ra = 440$) cases have become downwelling solutions while the other two cases are upwellings. One way of viewing these results, in the light of the simulations in which source boundary length was varied, is that varying the buoyancy parameter β in the Rayleigh number has a similar effect. This behavior can be interpreted in terms of a corresponding Rayleigh number.

5.5. Effect of Boundary Proximity

[41] Finally, the size of the modeled domain was varied to assess the impact of plume proximity to remote boundaries on upwelling or downwelling solutions. The domain height or width was changed in size by an amount that corresponded to an integer number of cell widths, so that the same discretization was used within the domain, which was then extended or truncated by some number of grid cells. The upper solute source boundary retained a width of 300 m (i.e., 150 m on the modeled half-domain).

[42] The results with the standard domain choice were compared with the following cases: (1) the width of the half-domain reduced from 300 m to 262.5 m, (2) the half-domain width increased to 337.5 m, (3) the domain height reduced from 150 m to 131.25 m, and (4) the domain height increased to 168.75 m. All cases result in an upwelling somewhat similar to that seen for the standard EVS problem of Figure 2. However, after the fourth simulation year, small differences appear. The outer plume is narrower when the domain width is reduced while the plume in the vertically extended domain grows longer, leading to lower concentration gradients in the bottom half of the domain at later times (Woods and Carey, manuscript in preparation, 2007).

[43] The effect of finite domain approximation and asymptotic far field boundary conditions is analyzed and studied numerically for a class of elliptic problems by *Carey and Seager* [1990]. Similar issues arise here in the context of long time simulations (e.g., 20 years) as the plumes approach remote boundaries. In practical applications with real finite boundary conditions (as in Elder's original experiment) the interaction is real and the plume structure may be impacted. In simulating field studies similar to the EVS porous medium problem, the domain may in reality be much larger but an artificial remote boundary may be chosen for convenience; in this case, automated domain extension would be a viable approach for assessing long-time plume behavior correctly.

6. Concluding Remarks

[44] The EVS problem is frequently used as a benchmark test for numerical codes simulating variable-density flow and transport within a saturated porous medium. As such, it illustrates many of the difficulties associated with simulating this type of flow. The problem is challenging because of its nonlinearity and is complicated by its steep initial concentration gradients and discontinuous boundary conditions. However, the nonlinearity is not unreasonable, as similar high Rayleigh numbers can occur in groundwater field sites. The steep gradients and discontinuous boundaries are less of an issue in the field, but may well occur in industrial processes or in laboratory studies using porous media. Thus the EVS problem is an example of the type of physical problem that one would expect a numerical code to be able to simulate reliably with due care.

[45] Despite this, there is now an extensive literature on the EVS problem which has yielded conflicting results on plume structure. Studies such as those by *Frolkovič and de Schepper* [2001] and *Johannsen* [2003] have led to the conclusion that there are several valid solutions for the problem. More generally there are mixed and conflicting results. This may limit the problem's usefulness as a benchmark, especially as the laboratory results of *Elder* [1967] are dated and not definitive. Clearly new experiments are needed and better numerical benchmarks may help guide experimental design. However, it is also clear that the EVS problem is a demanding test that has interesting numerical behavior, and a sensitive difficult test for simulation benchmark has its merits [*Anderson et al.*, 2005].

[46] We reason that a key issue to the underlying sensitivity relates to the width of the upper source concentration boundary. For the standard EVS problem, the length of the upper constant concentration boundary lies close to a critical transition regime between upwelling and downwelling cases. This can also explain the downwelling results of the smoothed boundary condition cases, as the smoothing effectively increases the length of the source boundary slightly and decreases the end effect, thereby modifying the source boundary influence and resulting in downwelling solutions for grid levels 6 and 7. As the EVS problem is set near a critical point in the source width and Rayleigh number, even small modeling or numerical perturbations may push the solution toward either of two nearby states if due caution is not exercised in controlling model approximation and simulation error.

[47] When using the EVS problem as a benchmark study, the modeler must be aware of the critical parameter values for this problem and that the behavior as a critical point is approached will be sensitive to perturbations in the mesh and other data. As a guideline, the problem should be run at an off-critical length first and then make similar simulations as the critical length is approached.

[48] **Acknowledgments.** The authors would like to thank Robert McLay, William Barth, and Benjamin Kirk of the University of Texas Computational Fluid Dynamics Laboratory for helpful discussions, software support, and technical assistance during this study.

References

Ackerer, P., A. Younes, and R. Mosé (1999), Modeling variable density flow and solute transport in porous medium: 1. Numerical model and verification, *Transp. Porous Media*, *35*, 345–373.

Analytic and Computational Research, Inc. (1994), *PORFLOW User's Manual Version 2.50*, Bel Air, Calif.

Anderson, M., W. Bangereth, and G. F. Carey (2005), Analysis of parameter sensitivity and experimental design for a class of nonlinear partial differential equations, *Int. J. Numer. Methods Fluids*, *48*, 583–605.

Barrett, R., et al. (1994), *Templates for the Solution of Linear Systems: Building Blocks for Iterative Methods*, 2nd ed., Soc. of Ind. and Appl. Math., Philadelphia, Pa.

Barth, B., and G. F. Carey (2006), On a natural convection benchmark problem in non-Newtonian fluids, *Numer. Heat Tranfer, Part B*, *50*, 193–216.

Bear, J. (1961), On the tensor form of dispersion, *J. Geophys. Res.*, *66*, 1185–1197.

Boufadel, M., M. Suidan, and A. Venosa (1999a), A numerical model for density-and-viscosity-dependent flows in two-dimensional variably saturated porous media, *J. Contam. Hydrol.*, *37*, 1–20.

Boufadel, M., M. Suidan, and A. Venosa (1999b), Numerical modeling of water flow below dry salt lakes: Effect of capillarity and viscosity, *J. Hydrol.*, *221*, 55–74.

Broadbridge, P., R. J. Moitsheki, and M. P. Edwards (2002), Analytical solutions for two dimensional solute transport with velocity-dependent dispersion, in *Environmental Mechanics: Water, Mass and Energy Transfer in the Biosphere*, *Geophys. Monogr. Ser.*, vol. 129, edited by P. A. C. Raats, D. E. Smiles, and A. Warrick, pp. 145–153, AGU, Washington, D. C.

Carey, G. F. (2006), A perspective on adaptive modeling and meshing (AM&M), *Comput. Methods Appl. Mech. Eng*, *195*, 214–235.

Carey, G. F., and M. Seager (1990), Adaptive domain extension and adaptive grids for unbounded sperically elliptic PDEs, *SIAM J. Sci. Stat. Comput.*, *11*(1), 92–111.

Carey, G. F., R. McLay, G. Bicken, B. Barth, S. Swift, and A. Ardelea (1999), Parallel finite element solution of three-dimensional Rayleigh-Bérnard-Maragoni flows, *Int. J. Numer. Methods Fluids*, *31*, 37–52.

Carey, G. F., W. Barth, J. A. Woods, B. Kirk, M. Anderson, S. Chow, and W. Bangereth (2004), Modeling error and constitutive relations in simulation of flow and transport, *Int. J. Numer. Methods Fluids*, *46*, 1211–1236.

Chandrasekhar, S. (1981), *Hydrodynamic and Hydromagnetic Stability*, Courier Dover Publ., North Chelmford, Mass.

Diersch, H.-J. (1996), *Interactive, Graphics-Based Finite-Element Simulation System FEFLOW for Modeling Groundwater Flow, Contaminant Mass and Heat Transport Processes: FEFLOW User's Manual Version 4.5*, WASY Ltd., Berlin.

Diersch, H.-J., and O. Kolditz (2002), Variable-density flow and transport in porous media: Approaches and challenges, *Adv. Water Resour.*, *25*, 899–944.

Elder, J. (1967), Transient convection in a porous medium, *J. Fluid Mech.*, *27*, 609–623.

Frolkovič, P., and H. de Schepper (2001), Numerical modelling of convection dominated transport coupled with density driven flow in porous media, *Adv. Water Resour.*, *24*, 63–72.

Gresho, P. M. and R. Sani (1998), *Incompressible Flow and the Finite Element Method: Advection-Diffusion and Isothermal Laminar Flow*, John Wiley, Hoboken, N. J.

Holzbecher, E. (1998), *Modeling Density-Driven Flow in Porous Media: Principles, Numerics, Software*, Springer, New York.

Horton, C. W., and F. T. Rogers (1945), Convection currents in a porous medium, *J. Appl. Phys.*, *16*, 367–370.

Johannsen, K. (2003), On the validity of the Boussinesq approximation for the Elder problem, *Comput. Geosci.*, *7*, 169–182.

Kolditz, O., R. Ratke, H.-J. Diersch, and W. Zielke (1997), Coupled groundwater flow and transport: 1. Verification of variable density flow and transport models, *Adv. Water Resour.*, *21*, 27–46.

Lapwood, E. (1948), Convection of a fluid in a porous medium, *Proc. Cambridge Philos. Soc.*, *44*, 508–521.

Lever, D. A. and C. P. Jackson (1985), On the equation for the flow of concentrated salt solution through a porous medium, *Rep. DOE/RW/85.100*, 2 pp., U.S. Dep. of Energy, Washington, D. C.

Mazzia, A., L. Bergamaschi, and M. Putti (2001), On the reliability of numerical solutions of brine transport in groundwater: Analysis of infiltration from a salt lake, *Transp. Porous Media*, *43*, 65–86.

Oldenburg, C. M., and K. Pruess (1995), Dispersive transport dynamics in a strongly coupled groundwater-brine flow system, *Water Resour. Res.*, *31*, 289–302.

Oltean, C., and M. A. Buès (2001), Coupled groundwater flow and transport in porous media: A conservative or non-conservative form?, *Transp. Porous Media*, *44*, 219–246.

Park, N. (1996), Closed-form solutions for steady state desnity-dependent flow and transport in a vertical soil column, *Water Resour. Res.*, *32*, 1317–1322.

Rayleigh, L. (1916), On convection currents in a horizontal layer of fluid when the higher temperature is on the under side, *Philos. Mag.*, *17*, 529–546.

Scheidegger, A. (1961), General theory of dispersion in porous media, *J. Geophys. Res.*, *66*, 3273–3278.

Simmons, C. T., and K. A. Narayan (1997), Mixed convection below a saline disposal basin, *J. Hydrol.*, *194*, 263–285.

Simpson, M. J., and T. P. Clement (2003), Theoretical analysis of the worthiness of Henry and Elder problems as benchmarks of density-dependent groundwater flow models, *Adv. Water Resour.*, *26*, 17–31.

Valliappan, S., W. Wang, and N. Khalili (1998), Contaminant transport under variable density flow in fractured media, *Int. J. Numer. Anal. Methods Geomech.*, *22*, 575–595.

van Duijn, C., and R. Schotting (1998), Brine transport in porous media: On the uses of Von Mises and similarity transformations, *Chem. Geol.*, *2*, 125–149.

Voss, C. I. (1984), SUTRA: A finite-element simulation model for saturated-unsaturated fluid-density-dependent ground-water flow with energy transport or chemically-reactive single-species solute transport, *Water Resour. Invest. Rep. 84-4369*, U.S. Geol. Surv., Washington, D. C.

Voss, C. I., and W. R. Souza (1987), Variable density flow and solute transport simulation of regional aquifers containing a narrow freshwater-saltwater transition zone, *Water Resour. Res.*, *23*, 1851–1866.

Woods, J. A., M. D. Teubner, C. T. Simmons, and K. A. Narayan (2003), Numerical error in groundwater flow and solute transport simulation, *Water Resour. Res.*, *39*(6), 1158, doi:10.1029/2001WR000586.

G. F. Carey, Institute for Computational Engineering and Sciences, University of Texas at Austin, Austin, TX 78712, USA. (carey@cfdlab.ae.utexas.edu)

J. A. Woods, Australian Water Environments, 1/198 Greenhill Road, Eastwood, SA 5063, Australia. (juliettewoods@austwaterenv.com.au)